Accepted Author Manuscript

Article Title: Multifunctional and sustainable soot modified nanofibrous membrane for adsorption, sensing and hydrogen peroxide electrogeneration

Authors: A.D. Alvarenga, M.H.M. Facure, I. Sánchez-Montes, G.O.S. Oliveira, M.R.V. Lanza, L.A. Mercante, D.S. Correa.

Journal: *Journal of Cleaner Production*., 422 (2023), 10.1016/j.jclepro.2023.138697

DOI: https://doi.org/10.1016/j.jclepro.2023.138697

Received: 10 May 2023
Acepted: 3 September 2023
Plublished online: 4 September 2023

Copyright Notice:

This is the accepted version of the following article: Alvarenga, M.H.M. Facure, I. Sánchez-Montes, G.O.S. Oliveira, M.R.V. Lanza, L.A. Mercante, D.S. Correa, Multifunctional and sustainable soot-modified nanofibrous membrane for adsorption, sensing and hydrogen peroxide electrogeneration, *Journal of Cleaner Production*, 2023, Article 138697, https://doi.org/10.1016/j.jclepro.2023.138697.

This version of the article has been accepted for publication, after peer review but is not the Version of Record and does not reflect post-acceptance improvements, or any corrections. The Version of Record is available online at: https://doi.org/10.1016/j.jclepro.2023.138697. Use of this Accepted Version is subject to the publisher's Accepted Manuscript terms of use: https://www.sciencedirect.com/journal/journal-of-cleaner-production/publish/open-access-options

© 2023 Elsevier Ltd. This manuscript is for non-commercial purposes only and must not be modified or enhanced by third parties.

Multifunctional and sustainable soot-modified nanofibrous membrane for adsorption, sensing and hydrogen peroxide electrogeneration

Augusto D. Alvarenga[a,b*], Murilo H. M. Facure[a,c], Isaac Sánchez-Montes[d], Géssica O. S. Oliveira[d], Marcos R. V. Lanza[d], Luiza A. Mercante[e], Daniel S. Correa[a,b,c*]

[a] Nanotechnology National Laboratory for Agriculture (LNNA), Embrapa Instrumentação, 13560-970 São Carlos, SP, Brazil

[b] PPG-Biotec, Center for Exact Sciences and Technology, Federal University of Sao Carlos (UFSCar), 13565-905 Sao Carlos, SP, Brazil

[c] PPGQ, Department of Chemistry, Center for Exact Sciences and Technology, Federal University of Sao Carlos (UFSCar), 13565-905 São Carlos, SP, Brazil

[d] Institute of Chemistry of São Carlos (IQSC), University of São Paulo (USP), 13563-120 São Carlos, SP, Brazil

[e] Institute of Chemistry, Federal University of Bahia (UFBA), 40170-280 Salvador, BA, Brazil

* Corresponding authors: augustoad2@yahoo.com.br; daniel.correa@embrapa.br

Abstract

The incineration of plastics and biomass is an efficient alternative to reduce the amount of solid waste and is also beneficial for energy production. Soot is one of the main byproducts generated during solid waste incineration, and so far, it has been treated as a pollutant. However, soot is an interesting nanostructured material displaying high specific surface area and chemical reactivity. In this work, soot produced by incomplete burning of plastic materials was combined with polymer nanofibers resulting in a multifunctional membrane explored for pollutant adsorption, sensing of organic pollutants, and in the electrogeneration of hydrogen peroxide. Specifically, soot was immobilized onto polyamide 6 nanofibrous membranes (NFM) produced by solution blow spinning following two different approaches: pre-synthesis and post-synthesis modification, and then the effect of soot chemical activation with NaOH was investigated. The adsorption tests showed that the chemical activation was essential to increase efficiency by improving its hydrophilicity and generation of adsorption sites. The experimental and calculated batch adsorption efficiency towards methylene blue was 94.33 mg/g and 37.71 mg/g, respectively. The adsorption efficiency in the fixed bed was 8.00 mg/g. The functional NFMs maintained their efficiency for at least ten adsorption cycles, increasing their economic viability. Furthermore, the NFMs were applied as flexible and free-standing electrodes for detecting methylene blue with a limit of detection of 2.4 nmol/L. The average per-electrode cost was estimated to be US$0.04. Finally, the NFM also demonstrated the ability to generate H_2O_2 *in situ*. Altogether, these results suggest that the immobilization of soot onto nanofibrous membranes is an efficient strategy for developing multifunctional and sustainable materials towards environmental applications.

Keywords: sustainability, adsorption, sensor, hydrogen peroxide generation, soot, nanofibers.

Graphical Abstract

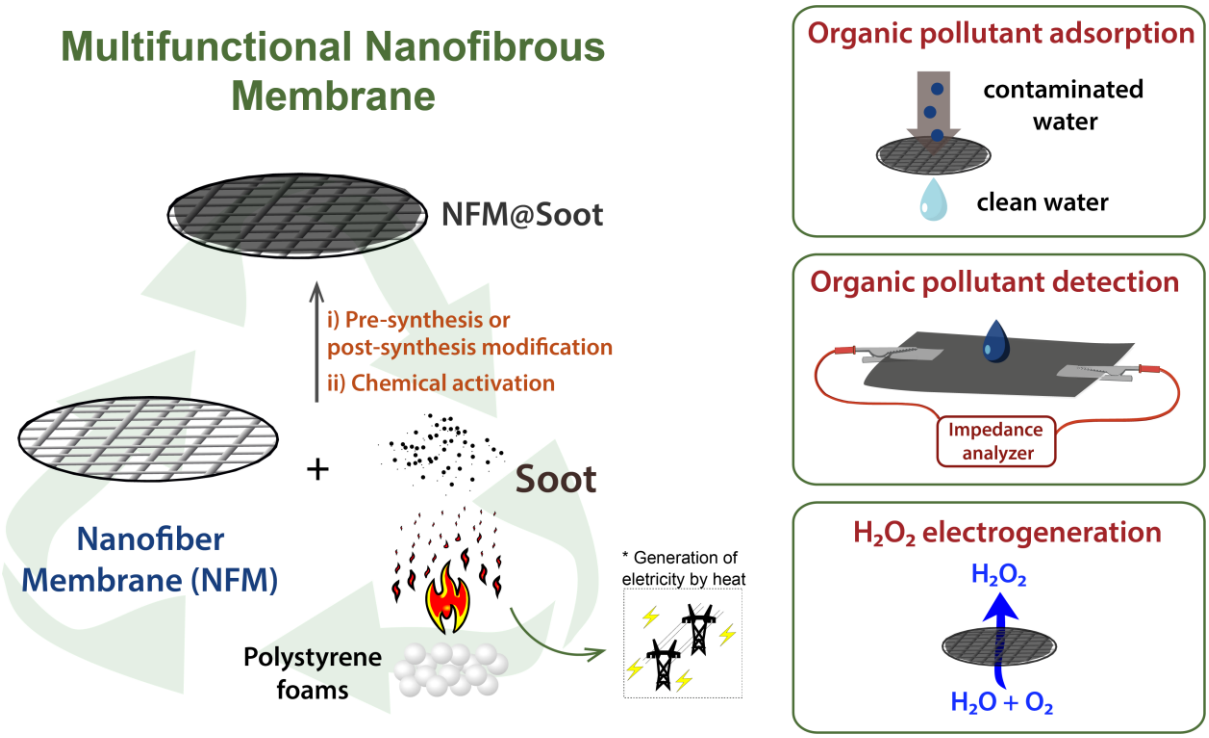

1. Introduction

Multifunctional platforms have gained significant attention in recent years due to their versatility and ability to perform multiple tasks simultaneously (Yuan et al., 2020). In particular, multifunctional platforms that can remove and sense pollutants from water are important in a scenario of population growth combined with higher levels of consumption of natural resources have compromised global sustainability (Wang et al., 2022). Consequently, there is a need to develop novel technologies based on abundant, cheap, and sustainable resources (Neolaka et al., 2023b; Quina et al., 2018). Soot (Du and Li, 2019) is an example of such a resource, which production process is characterized by the incomplete burning of materials as fuels (Long et al., 2013). Soot is considered to be toxic mainly because it can be related to the development of cancer and cardiovascular disease, and thus, it is important to its collection at the source of production (Kirrane et al., 2019). Despite these problems, these materials have tunable and interesting characteristics for developing new technologies. In addition, the incineration of materials is the most efficient way of reducing inorganic waste, allowing energy recovery (Yao et al., 2019). The creation of technologies involving carbon is in accordance with the objectives of reducing the effects of global warming (Yao et al., 2019).

Soot is characterized by being rich in organic carbon in a complex mixture of different organic compounds, such as polycyclic aromatics hydrocarbons (PAHs), among others, which tend to agglomerate (Saini et al., 2021). This interaction is influenced by several parameters, including particle size, molecular weight, vapor pressure, and the solvent (Long et al., 2013; Michelsen, 2017; Saini et al., 2021). The physical and chemical properties of soot depend on the raw material and the carbonization conditions that will influence its purity, chemical structure, and molecular conformation (Michelsen, 2017; Pahalagedara et al., 2012), which in turn will affect characteristics such as hydrophilicity/hydrophobicity (Shen et al., 2016) and thermal and electric conductivity (Byamba-Ochir et al., 2016). Furthermore, these characteristics can be manipulated to achieve specific characteristics for applications in electronics (Wan et al., 2020), supercapacitors (Wang et al., 2021), batteries (L. Li et al., 2021), health (Wan et al., 2020), and water treatment (Ali et al., 2019). Among these applications, purification and detection of pollutants in water are contemporaneously necessary. The availability of drinking water has decreased due to the increase in demand and pollution. Soot is used in water treatment through oil and water separation, adsorption (Kumar Sahoo et al., 2020) process, filtration (Trubetskaya et al., 2019), catalysis (Zhang et al., 2015), and sensing (Sabri et al., 2018) of pollutants. Adsorption process is particularly interesting to remove

resistant organic pollutants due to its easy operation, versatility, low energy consumption and low cost (Neolaka et al., 2023a). In this process, the high surface area is a desired characteristic. Often these applications are carried out with pure soot (Kumar Sahoo et al., 2020). Thus, the immobilization of soot in nanofibers is an interesting, but yet little-explored alternative (Saini et al., 2021).

Among nanofibrous carriers, solution blow spun nanofibrous membranes with porous structures have exhibited significant potential owing to their large surface area, inter-fiber porosity, small fiber diameters and suitable mechanical strength. These properties ensure enhanced nanomaterial loading, recycling, and reusability. With this perspective in mind, our work demonstrates the utilization of soot as an effective modifier for nanofibrous membranes, leading to the development of cost-effective multifunctional composite materials. Specifically, polyamide 6 (PA6) nanofibers produced by solution blow spinning (SBS) technique were modified with soot using two low-cost and scalable approaches: pre- and post-modification. The modified nanofibers were then chemically activated with NaOH, enabling their multifunctional application in adsorption and sensing of organic molecules as well as in situ generation of hydrogen peroxide (H_2O_2), as illustrated in Scheme 1. Notably, the multifunctional behavior of soot-functionalized nanofibrous membranes has received limited attention in the literature, making our study a significant contribution to the field. Furthermore, the use of soot obtained from burning polystyrene for the intended environmental applications represents a novel and promising approach with distinct advantages.

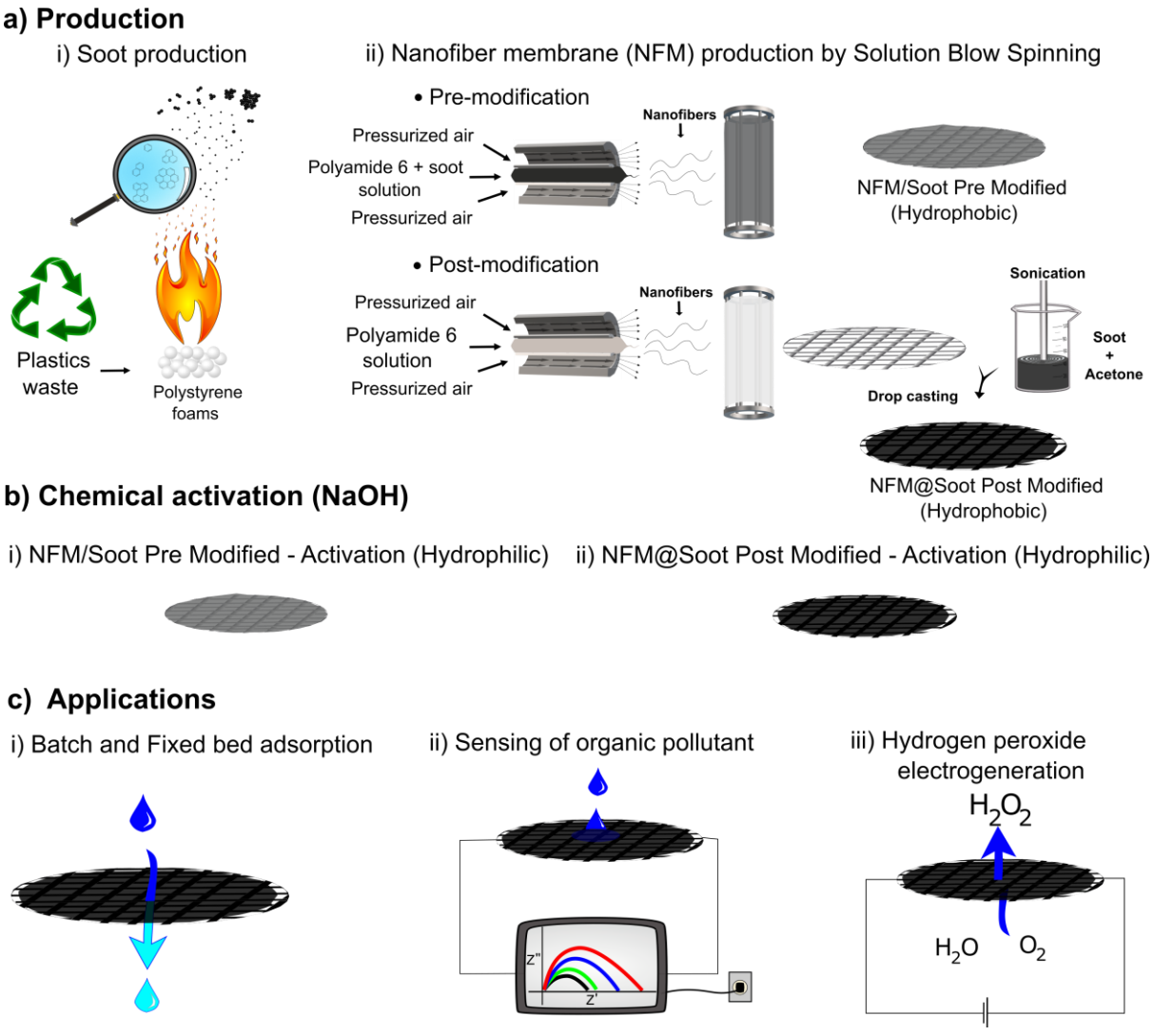

Scheme 1: Schematic illustration of the production of a) NFMs made of PA6 and Soot, b) chemical activation and c) applications in (i) adsorption, (ii) sensing of organic pollutant, and (iii) hydrogen peroxide electrogeneration.

2. Experimental

Polyamide 6 (PA6) was purchased from Sigma Aldrich. Formic acid and acetone were acquired from Synth Chemical (Brazil). Dichloromethane and NaOH were purchased from LSChemicals (Brazil) and Chemical Moderna (Brazil), respectively. The methylene blue (MB) was purchased from NEON (Brazil). All the chemicals were used as received.

The soot was produced by burning polystyrene waste, which was originally employed as polystyrene foams to protect household appliances. The soot was collected by an aluminum plate. The physicochemical characterization of soot is shown in Supplementary Material (Fig. S1).

2.1 Preparation of PA6 NFMs by SBS method

First, a solution of PA6 (25% w/v) in formic acid/dichloromethane (3:2, v/v) was produced under stirring for 3 h at room temperature (25 °C). The homogeneous solution was transferred to a 20 mL glass syringe to start the nanofiber production process using the SBS apparatus. This apparatus consists of an ejector pump (model NE-300, SyringerPump), a source of compressed air, a concentric nozzle system and a rotating rod collector. The PA6 nanofiber membrane was obtained using an ejection rate of 5 mL/h, air pressure of 2 bar (200 kPa), a collector rotation speed of 180 rpm, and a working distance of 30 cm. Nanofibers were produced at room temperature (25 ± 3 °C) in a relative humidity of 35 ± 5 %. After synthesis, the PA6 membranes were kept in an oven at 50 °C overnight to ensure the evaporation of residual solvents(Alvarenga et al., 2023; Alvarenga and Correa, 2021).

2.2 Preparation of PA6 NFMs modified with soot

The soot produced by the combustion of polystyrene was used in the modification of PA6 NFMs following two different approaches: pre-synthesis and post-synthesis modification. The soot recovery rate was about 1.7% of the mass of the combusted polystyrene.

2.2.1 Pre-synthesis modification

In the pre-synthesis modification, 1% (0.025 g) and 3 % (0.075 g) of soot (in relation to PA6) was first dispersed in formic acid along with the PA6 pellets, and then dichloromethane was added to the dispersion. The NFM/Soot1% (NFM/S1%) and NFM/Soot3% (NFM/S3%) were prepared using the same parameters to produce neat PA6 fibers.

2.2.2 Post-synthesis modification

The post-synthesis modification was carried out by the dip-coating technique. Firstly, the freshly produced soot was dispersed in acetone by ultrasonic probe sonication (Branson Digital Sonifier SFX 550, 550 W) with 30% amplitude for 15 min. Subsequently, the PA6 NFMs were dipped into approximately 14 mL of the soot suspension (3 mg/mL). Volumes smaller than 14 mL did not provide complete coverage of the NFMs. Finally, the membranes were kept in an oven at 50 °C overnight. This membrane was named NFM@S.

2.2.3 Chemical activation

The modified NFMs were chemically activated by treatment with 1 mol/L NaOH solution for 3 h. Then, the NFMs were washed with three baths of Milli-Q water and dried at 50 °C for 24 h. After activation, the membranes were called NFM/S1%-A, NFM/S3%-A, and NFM@S-A. Table 1 summarizes the samples produced and their acronyms.

Table 1. Abbreviations of the samples produced.

Synthesis method	PA6 NFMs modified with soot	NFMs modified with soot and activated with NaOH
NFM pre-modified (soot in PA6 solution)	NFM/S1%	NFM/S1%-A
	NFM/S3%	NFM/S3%-A
NFMs post-modified (dip-coating)	NFM@S	NFM@S-A

Abbreviation: NFMs = Nanofibrous membranes; PA6 = Polyamide 6

2.3 Characterization

The specific surface area, pore size and volume of soot were characterized by Brunauer–Emmett–Teller (BET) (Micrometrics ASAP-2020). The zeta potential and particle size of soot in water solution were characterized by a Zetasizer Nano ZS (Malvern Instruments).

The morphology of soot and NFMs were evaluated by Scanning Electron Microscopy (SEM) (JEOL JSM-6510) and Field Emission Scanning Electron Microscopy (FE-SEM) (JSM-6701F JEOL). Energy Dispersive X-Ray Spectroscopy (EDS) (JEOL JSM-6510) was carried out to evaluate the chemical composition of soot and NFMs.

Fourier transform infrared (FTIR) spectra of NFMs and soot were collected in ATR mode from 400 to 4000 cm^{-1} using a Bruker Vertex 70 equipment with a total of 32 scans with a resolution of 4 cm^{-1}. The X-ray diffraction (XRD) was performed with a Shimadzu XRD-6000 diffractometer using 30 kV and 30 mA (Cu Kα radiation).

Thermogravimetric (TGA) analyses of NFMs were carried out using a Q500 TA instrument. The samples were placed in platinum pans and analyzed under a mixture (40:60) of nitrogen:air at a flow rate of 10 °C min^{-1} from room temperature up to 600 °C.

The tensile tests of NFMs were performed with a DMA Q800 equipment in tension mode equipped with a thin film clamp. The NFMs with thickness of nearly 0.170 mm were cut

into regular shapes measuring 6.14 mm wide, and 52 mm length and tensile tests were carried out in uniaxial tension with ramp of 700 µm min^{-1}, preload force of 0.001 N and strain amplitude of 0.1% at 29 °C.

Contact angle measurements of the NFMs and soot were performed with a goniometer equipped with a Biolin Scientific Attention Theta Lite dripping 5 µL of ultrapure water on the NFMs and the angle was calculated by the KSV CAM 2008 software (system CAM 101 model KSV Instruments).

Point zero charge (PZC) was determined with NaCl solution (10 mL; 0.01 mol/L) with pH values ranging from 1 to 12. The pH was adjusted using 0.1 mol/L NaOH and 0.1 mol/L HCl solutions. Then, about 10 mg of NFM/S3%-A and NFM@S-A were immersed in each solution with a different pH and stirred for 12 hours at 25°C. The pH solution was measured after removing the NFMs. The PZC value was obtained by plotting the pH values versus the initial pH (Neolaka et al., 2022).

2.4 Applications

2.4.1 Dye adsorption

Batch and fixed bed adsorption tests were performed to evaluate the adsorption capacity and kinetics of the membranes. Methylene Blue (MB), a cationic dye widely employed in textile industries, was chosen as the target molecule for this study due to its remarkable affinity for adsorption onto solids, ease of monitoring, and the opportunity it provides for meaningful comparisons with the extensive body of scientific literature available on this subject (Santoso et al., 2020). The concentrations of the MB solutions were measured using a UV-vis spectrophotometer (Shimadzu/UV-1900) collecting the absorbance values at 665, which calibration curve is shown in Fig. S2. Batch adsorption tests were performed in a 25 mL MB solution using a membrane mass ranging from 5 to 20 mg. Global and relative efficiency were evaluated according to Eq. S1 and Eq. S2, respectively, as shown in Table S1. Kinetics tests evaluate the rate of adsorption as a function of time and are important to quantify mass transfer. The kinetic tests were performed by removing aliquots of the MB solution at regular intervals, measuring their absorbance immediately, and returning the aliquot to the solution. The results were evaluated according to the pseudo 1° order (Eq. S1 3 – physisorption predominant) (Lagergren, 1898) and pseudo 2° order (Eq. S4 – chemisorption predominant) (Blanchard et al., 1984) models.

The isothermal tests were carried out by soaking 10 mg of the NFMs in 25 mL of MB solution (5 to 200 ppm) for about 12 h. The results were evaluated according to Freundlich (Eq. S5) (Freundlich, 1906) and Langmuir (Eq. S6 and Eq. S7) (Langmuir, 1918) isothermal models. The equilibrium parameter Langmuir model as calculated with Eq. S7.

Fixed bed adsorption tests are important to evaluate the rate of adsorption in continuous systems to design systems for real applications (Ye et al., 2019). Here the NFMs were submitted to filtration tests with 10 mg/L solutions of MB varying the flow rates (1 mL/min). Total and relative efficiency were calculated using Eq. S8 and Eq. S9, respectively. The results were evaluated according to the Bohart Adams model (Eq. S10).

The reuse tests were carried out in a fixed bed using ~ 30 mg of NFMs. First, the NFMs were subjected to 2 ml of MB solution (10 mg/L) at 1 ml/h followed by the passage of 2 ml of commercial ethanol for desorption.

Theoretical details of the models employed here can be found elsewhere (Bohart and Adams, 1920; Bonilla-Petriciolet et al., 2017; Chu, 2020; Lagergren, 1898; Langmuir, 1918; Tran et al., 2017; Yuh-Shan, 1995). The equations are presented in the supplementary file.

2.4.2 Dye detection

The NFMs were used as sensing electrodes in electrical impedance measurements. The nanofibers were cut in dimensions of 1 cm × 2 cm and used to evaluate MB solutions at different concentrations, ranging from 10 nmol/L to 10 mmol/L. The electrical impedance measurements were performed using a Solartron impedance analyzer (1260A), which data were collected in the frequency range from 10 MHz to 1 Hz. Measurements were carried out in triplicate by dropping 0.7 µL of MB solution onto the membrane and the electrical resistance values extracted from the real part of impedance data were treated by multidimensional projection techniques using the PEx-Sensors software (Paulovich et al., 2007).

2.4.3 H_2O_2 electro-generation

The electrochemical measurements of NFMs were conducted using linear sweep voltammetry (LSV) and cyclic voltammetry (CV) using potentiostat/galvanostat (Metrohm Autolab PGSTAT-128N). The membrane (exposed area of 20 cm^2) was coupled to the bottom of a one-compartment three-electrode cell (Barros et al., 2013) to act as a gas diffusion electrode (GDE) (cathode or working electrode) and a platinized titanium was used as anode

(or counter electrode), and Ag/AgCl (3 mol/L KCl) as the reference electrode. The LSV was performed at a scan rate of 10 mV/s and potential interval of 0 to -2.0 V and the CV at a scan rate of 50 mV/s and potential interval of -1 to -1.2 V. The electrolyte used was 0.1 mol/L K_2SO_4 solution (pH ~near neutral without adjustment). To evaluate the feasibility of the membrane in the H_2O_2 electrogeneration, a current density of 25 mA/cm^2 was applied during 90 min electrolysis (same system and electrolyte used in the electrochemical characterization). A continuous flow of O_2 was continuously injected into the electrolyte from the bottom of the electrochemical cell at a flow rate of 50 mL/min during all measurements. All the experiments were performed using 100 mL of 0.1 mol/L K_2SO_4 under mechanical stirring at 20 °C by using a thermostatic bath.

The peroxymolybdate method was used to quantify the H_2O_2 accumulated in the system. Thus, 0.5 mL aliquots of the electrolyte were collected at different electrolysis times and mixed with 4 mL of a solution of $(NH_4)_6Mo_7O_{24}$ ($2.4x10^{-3}$ mol/L) in H_2SO_4 (0.5 mol/L), which allows the detection of the absorbance at 350 nm. A Shimadzu UV-1900 UV-Vis spectrometer was used for the measurements (Forti et al., 2007).

2.5 Cost estimation

The production process of the NFMs was mapped for cost estimation according to life-cycle cost analysis (Pryce et al., 2022). Energy and raw materials costs were used as input to the analysis. Logistics, storage, infrastructure, equipment, and disposal costs were disregarded in the cost analysis. The cost analysis is presented in the supplementary file (Figures S3 and S4, and Tables S2 and S3).

3. Results and discussion

3.1 Characterization of NFMs modified with soot

The morphology of the NFMs was evaluated by SEM images, shown in Fig. 1 and Fig. S5. The NFM/S3% and NFM@S images were taken at different magnifications to show the morphological details of the soot after the pre- and post-synthesis immobilizations process. It can be noted that different immobilization methods led to different soot morphologies. The NFM/S3% (Fig. 1a) have regions where the soot can be seen as a veil, similar to that observed in graphene structure (Kumar Sahoo et al., 2020). The NFM@S (Fig. 1b) shows a greater

amount of soot agglomerated on the nanofiber's surface, which appears to be entirely coated by the soot. After the chemical activation, no significant morphological changes in NFM/S3%-A (Fig. 1c) were observed. On the other hand, the NFM@S-A (Fig. 1d) after activation has a more discontinuous surface, with some pores in the coating. In stability tests by immersion under agitation and under water flow in a fixed bed, the NFMs remained stable without releasing soot. The SEM image of the NFM/S1% reveals that the soot is not evident at the surface of the nanofibers, which may indicate its presence in the fiber bulk (Fig. S6). Tensile testing revealed that NFM@S exhibited higher tensile strength compared to other NFMs. Nevertheless, this performance was influenced by the activation process. Notably, NFM/S3% did not experience a reduction in tensile strength post-activation. A more detailed discussion is addressed in the supplementary materials (Fig. S7 and Fig. S8). XRD analysis shows that the soot remains amorphous in the nanofibers (Fig. S9). TGA analysis (Fig. S10) shown the NFM/S1%, NFM/S3% and NFM@S have about 10%, 15% and 40% soot in their composition.

Contact angle measurements were performed to assess the interaction of NFMs with water. NFM/S1% and NFM/S3% present similar contact angle behaviors, with an initial angle of 123° (detail in Fig. 1a), which is decreased to 0° in 2 min. The NFM@S showed hydrophobic behavior with a constant contact angle at 141° (Fig. 1b) (Singh et al., 2019). After activation with NaOH, NFM/S3%-A exhibited an angle of 0° after 20 seconds (details in Fig. 1c). The NFM@S-A presented a dubious behavior (Fig. 1d). There were regions where the contact angle changed to 0° in about 20 seconds and there were tests where the angle stabilized around 70°. The increase in the hydrophilicity of the NFMs may be due to the oxygenation of the soot, improving its interaction with water (Alvarenga et al., 2023; Zhao et al., 2016). Specifically, for the NFM@S-A, their dubious behavior may indicate that the chemical activation that acts superficially on the soot agglomerates was not homogeneous throughout the NFM surface.

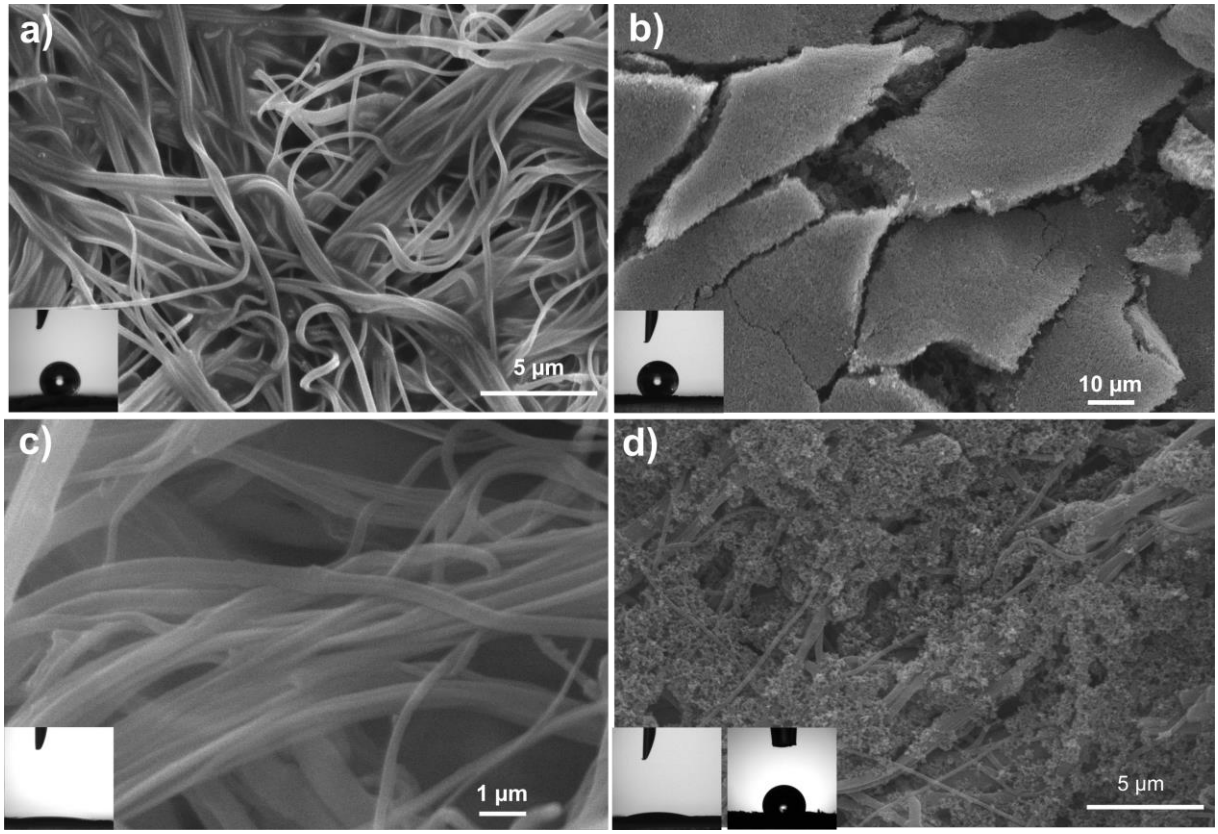

Figure 1. SEM images of a) pre-modified NFM/S3%, b) post-modified NFM@S, c) NFM/S3%-A activated, d) NFM@S-A activated and detail of the contact angles of the respective NFMs.

The FTIR of the NFMs is shown in Fig S11. The presence of soot in NFMs was not so evident by FTIR. After activation, it is possible to observe the appearance of a peak at 850 cm^{-1}, which is representative of anhydrides, suggesting that activation promotes soot oxidation (Alvarenga et al., 2023; Zhao et al., 2016). The surface chemical properties of NFMs before and after activation were investigated by XPS and are displayed in Table 3. NFMs/S3% showed a higher oxygenation level, which is attributed to the oxygen present in the PA6 molecule, since soot coverage is not complete, as seen in Fig. 1a and c. On the other hand, the NFMs@S presented a greater soot coating, which may explain a lower surface oxygenation level. Chemical activation led to the surface oxygenation of both NFMs as expected (Byamba-Ochir et al., 2016; Zhao et al., 2016).

Table 3. XPS NFMs analysis before and after chemical activation.

	C%	C=C	C-C	O% total	C-O	C=O	O-C=O

	total						
NFM/S3%	71.43	28.29	71.71	28.57	27.29	56.06	16.65
NFM/S3%-A	56.79	26.37	73.63	43.21	29.55	54.96	15.52
NFM@S	86.20	48.83	51.17	13.79	49.55	38.51	11.94
NFM@S-A	75.68	45.10	54.90	24.32	10.58	78.82	10.60

Raman analyzes were performed to compare the proportion of sp^2 (corresponding to G band at 1580 cm^{-1}) and sp^3 (corresponding to D band at 1340 cm^{-1}) binding on the surface of the NFMs. The NFM/S3% presents a higher proportion of sp2-hybridized carbon as observed in Fig. 2a (Pahalagedara et al., 2012; Yan et al., 2019). After activation (Fig. 2b,c) a peak intensity inversion between the G and D bands was observed, indicating a decrease in the number of double bonds between carbons (Byamba-Ochir et al., 2016). This fact can be explained by the soot oxidation during the chemical activation, as observed in other works (Byamba-Ochir et al., 2016; Pahalagedara et al., 2012; Yan et al., 2019) and corroborated by the XPS analysis. It was not possible to measure the NFM@S sample signal due to the high degree of luminescence coming from PHAs on this surface. NFM@S-A showed a higher proportion of sp2-hybridized carbon even after activation. This fact can be explained by the high degree of soot crystallinity organized in layers forming a sphere, as observed in Fig. S1b (He et al., 2021; Michelsen, 2017; Saini et al., 2021; Sirignano et al., 2016).

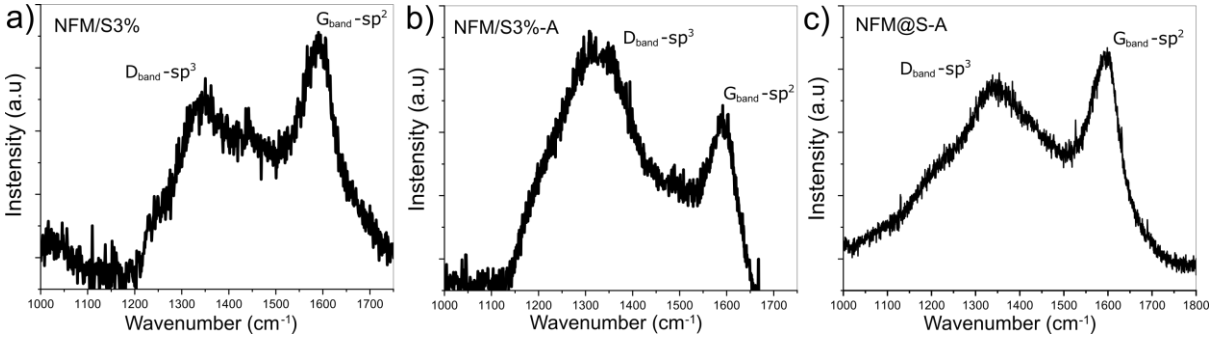

Figure 2. Raman analysis of a) NFM/3%, b) NFM/3%-A and NFM@S-A.

3.3 Applications of NFMs

3.3.1 Adsorption and filtration studies using NFMs with soot

The MB adsorption efficiencies of the NFMs were evaluated in batch and fixed bed. Preliminary tests were performed with ~10 mg of NFMs in 25 mL of 10 mg/L MB solutions for 12 hours. The activation increased the relative efficiency of adsorption from 0.63 (7.4 %) and 1.74 mg/g (20.4%) to 6.83 (41.4%) and 13.92 mg/g (83.4%) for NFM/S1%-A and NFM/S3%-A, respectively. NFM@S did not present adsorption capacity due to its hydrophobic behavior. After activation, NFM@S-A showed an adsorption capacity of 8.53 mg/g (49.0%). This efficiency gain is attributed to the oxygenation of carbonic structures, which can enhance the interaction with water and MB cationic dye (Alvarenga et al., 2023).

The adsorption kinetics of NFM/S3%-A and NFM@S-A were also evaluated. In Fig. 3a, all NFMs show rapid adsorption up to 100 min followed by a drop in the adsorption rate. The best correlation with the pseudo 2° order model in both NFMs indicates that chemisorption is the predominant factor in adsorption (Table S4). The adsorption kinetics influences the fixed bed adsorption efficiency (Alvarenga et al., 2023; Alvarenga and Correa, 2021).

Fig. 3b and 3c shows the adsorption efficiencies of NFM/S3%-A and NFM@S-A at different initial MB concentrations, respectively. Removal efficiency decreased with increasing MB solution concentration due to depletion of adsorption sites. The maximum experimental capacities of NFM/S3%-A and NFM@S-A were found to be 94.33 mg/g and 74.91 mg/g, respectively. However, isothermal tests revealed significant variation in relative efficiencies. This phenomenon can be attributed to non-homogeneous activation resulting from soot agglomeration and its inherent hydrophobic behavior. The maximum efficiencies calculated for NFM/S3%-A and NFM@S-A were 37.71 mg/g and 36.38 mg/g, respectively. Relative efficiency (q_e) decreased at concentration above 200 mg/L, suggesting a stronger interaction between MB molecules at high concentrations solutions rather than between MB and adsorption sites (Bonilla-Petriciolet et al., 2017). Fig. 3d, Fig. 3e and Fig S12 illustrate the values obtained from experimental tests. The higher relative efficiency of NFM/S3%-A compared to NFM@S-A can be attributed to the increased exposure of adsorption sites, resulting from reduced soot agglomeration (which would otherwise block the sites) and enhanced hydrophilicity (Fig. 1). NFMs without chemical activation exhibited inferior adsorption performance. For instance, NFM@S demonstrated negligible adsorption capacity due to its hydrophobic nature, while NFM/S3% exhibited a relative efficiency of only 12.11 mg/g (q max: 12.17 mg/g). These performance discrepancies can be attributed to the changes in hydrophilicity induced by NFM activation and soot oxidation, as supported by contact angle and XPS analyses. Nevertheless, further research on improved dispersion and chemical

activation methods for achieving a more homogeneous soot distribution is warranted to enhance its pollutant adsorption performance.

Table S5 also compares the adsorption efficiencies of the NFMs developed here with other works that employ soot as an adsorbent of MB. It is worth mentioning that pure PA6 NFMs do not present any adsorption capacity, corroborating that the soot contained onto the NFMs is responsible for the membranes' adsorption capability. Despite this, the mass of PA6 was not disregarded in the efficiency calculations, as it is important as a soot immobilization matrix. In other works reported in the literature, soot was used immobilized on micrometric surfaces (Nwafor et al., 2021; Pratap Singh and Vaish, 2020) or as a free material (Singh and Vaish, 2020; Wang et al., 2008), which can lead to agglomeration and loss of efficiency. Our results indicate that soot can be immobilized by the pre synthesis method on nano-sized surfaces, increasing its exposed surface area and thus enhancing the adsorption efficiency. Despite this, controlling soot agglomeration is still a challenge that, when overcome, can bring greater gains in adsorption efficiency. In addition, the immobilization on the NFM's surface allowed the chemical activation in water to occur efficiently, which was not possible with isolated soot due to its high hydrophobicity. Investigations in the chemical manipulation of immobilized soot can also bring performance gains.

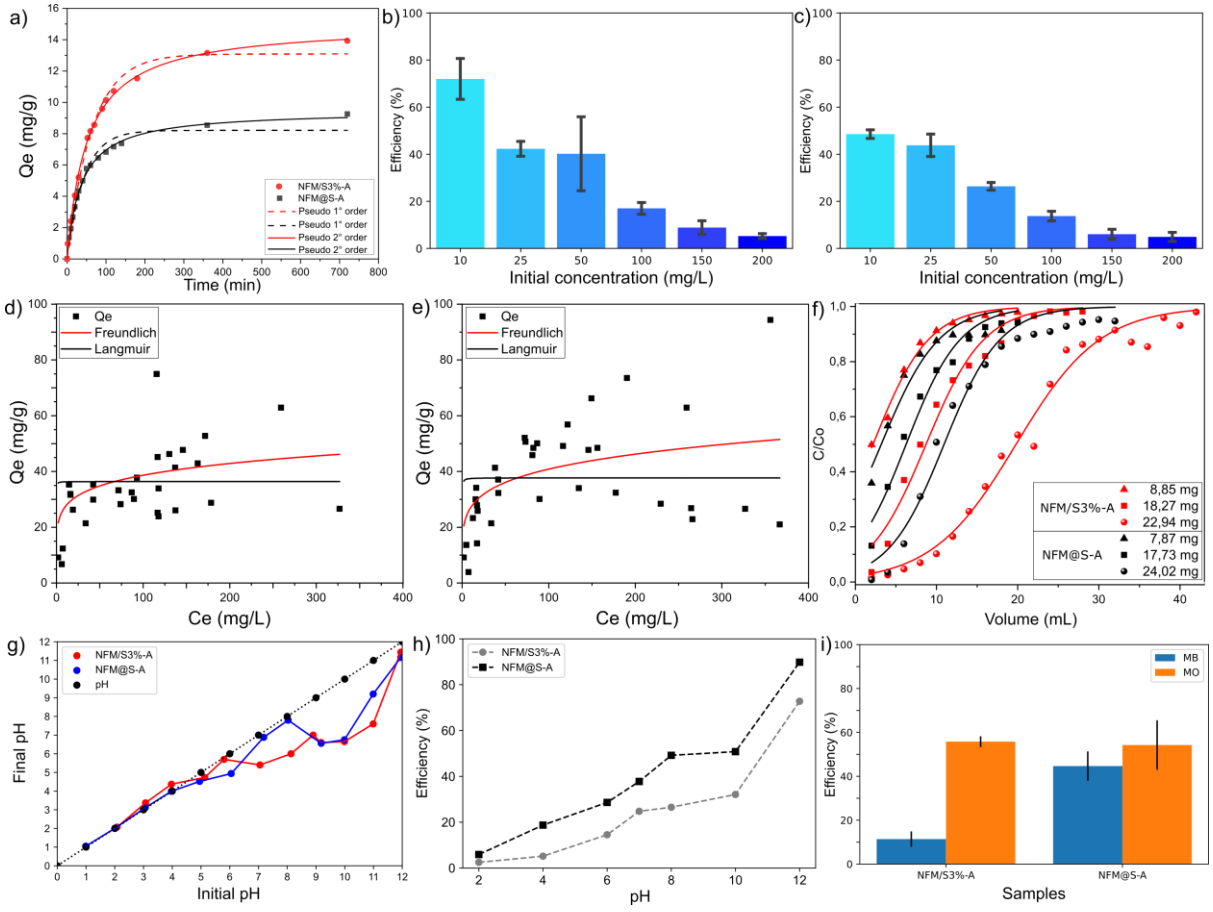

Figure 3. a) Adsorption kinetics of NFM/S3%-A and NFM@S-A. Efficiency of b) NFM/S3%-A and c) NFM@S-A at different initial concentrations of the MB solution. Adsorption isotherms of d) NFM/S3%-A and e) NFM@S-A. f) fixed bed adsorption of NFMs, g) PZC, h) adsorption efficiency of MB at different pH and i) adsorption of MO as interferent.

Fixed bed tests were performed with NFM@S-A and NFM/S3%-A to evaluate the performance of membranes in continuous filtration systems, which results are shown in Fig. 3f. Larger NFM masses led to larger breakthrough volumes due to the increase in available adsorption area. The pre-modified membranes performed better in the same way in the batch adsorption tests. The NFM/S3%-A with masses of 8.85 mg, 18.27 mg, and 22.94 mg yielded relative efficiencies of 2.90 mg/g, 4.14 mg/g, and 8.00 mg/g, respectively. The NFM@S-A with masses of 7.87 mg, 17.73 mg, and 24.02 mg yielded relative efficiencies of 1.47 mg/g, 1.77 mg/g, and 2.15 mg/g, respectively. The drop in relative efficiency between batch adsorption and fixed bed adsorption tests is explained by the shorter residence time of the solution in the adsorption system (Alvarenga and Correa, 2021; Jiang et al., 2020; Zhao et al., 2019). Besides, the decrease in efficiency of each NFMs in relation to the NFM mass decrease is explained by the greater possibility of the solution finding preferential flow channels in thinner NFMs.

The PZC value of NFM/S3%-A and NFM@S-A were identified in pH ranging 1 to 5 (Fig. 3g). This means that the adsorption of cations will be facilitated above this pH. To verify the influence of pH on MB adsorption, 10 mg of NFMs were added to 25 mL of MB solution (10mg/L) at different pH (2, 4, 6, 7, 8, 10 and 12) (Fig. 3h). As expected, solutions with a pH below PZC (pH=5) presented low adsorption efficiency while solutions with higher pHs increased efficiencies, reaching a maximum efficiency at pH 12 (Neolaka et al., 2021).

MO was employed to study the influence of anionic interferents (Fig. 3i) (Neolaka et al., 2018). Surprisingly, about 50% was removed by both NFMs. This fact is explained by the π=π interaction between the MO dye molecule and the round soot rings or O-π interaction by electrostatic interaction or H-bonding complexations (Fig. S13) (Karthikeyan et al., 2021).

To investigate the adsorption mechanism of MB onto NFMs, FTIR analyses were conducted before and after adsorption (Fig. S14). The FTIR band intensity decrease at around 3500 and 3000 cm^{-1} (O-H) and 1400 cm^{-1} (C-O) suggesting the adsorption of MB through electrostatic and intermolecular interactions (S. Li et al., 2021).

The conditioning of NFMs in commercial ethanol was also evaluated to enhance the adsorption performance, as observed in our previous work (Alvarenga and Correa, 2021).

NFM@S-A conditioned in ethanol increased the adsorption capacity from 2.13 mg/g to 3.86 mg/g. This conditioning promotes the adsorption of ethanol on porous carbon structures that enhances the interaction with MB. On the other hand, the same behavior is not observed for NFM/S3%-A, once in this case the soot is in graphene-like sheet forms.

Reuse tests of NFM/S3%-A and NFM@S-A were performed (Fig. 4), and in the case of NFM/S3%-A, the adsorption capability dropped from 98% to nearly 39% in the 6th cycle and remained stable until the 10th cycle. Desorption was around 70%. The NFM@S-A maintained a performance of nearly 99% until the 10th cycle and the desorption tended to increase. This situation may be related to the higher adsorption energy of NFM/S3%-A with MB in relation to NFM@S-A, making its desorption difficult and thus impairing its performance in reuse tests. Thus, lower adsorption energy of MB with NFM@S-A facilitates desorption, releasing adsorption sites in subsequent cycles. Furthermore, the interaction of ethanol with soot from NFM@S-A can adsorb on the surface of the porous carbon structure, increasing the MB adsorption efficiency, as observed in our previous work (Alvarenga and Correa, 2021). The same behavior was not observed for NFM/S3%-A due to the soot being in the form of sheets like graphene, preventing the adsorption of ethanol.

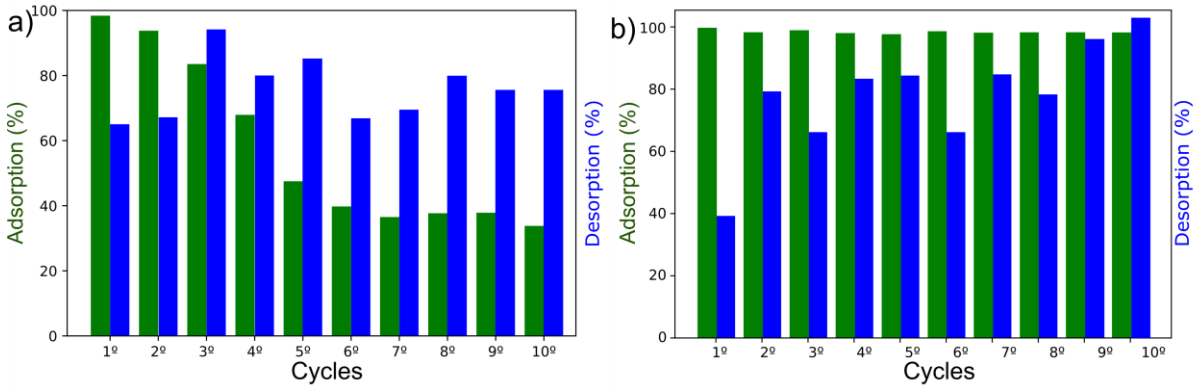

Figure 4. a) Reuse in of a) NFM/S3%-A and b) NFM@S-A with adsorption represented by green bars and desorption by blue bars.

3.3.2 Detection of MB concentration by impedance spectroscopy analysis

The NFM@S-A were also used as flexible and free-standing electrodes in electrical impedance spectroscopy measurements for the analyses of different concentrations of MB solutions. NFM/S3% was not used in these tests due to their electrical insulating characteristic due to the discontinuous presence of soot (Fig. 1a, c). The obtained experimental data were treated using the Principal Component Analysis (PCA) (Ringnér, 2008), as shown in. Fig. 5a.

Specifically, the PCA plot was obtained using the electrical resistance values collected over the frequency range from 1 MHz to 10 Hz. The frequencies were selected using the Parallel Components analysis, which indicates if the data obtained at a given frequency contributes to the discrimination analysis (Andre et al., 2020). The results obtained with the parallel Components analysis (Fig. S15a) show that the NFM@S-A electrode responds well at all frequencies studied since the blue boxes obtained indicate the relevance of the data collected in that particular frequency (Andre et al., 2020). Fig. S15b shows a photograph of the apparatus used to fix the NFM during the impedance measurement.

The PCA graph (Fig. 5a) shows that the use of the NFM@S-A membrane was able to differentiate samples of MB solutions with distinct concentrations. The PCA accounts for 99.85% (PC1 + PC2) of the variance, indicating a good correlation between the data (Facure et al., 2017). It is worth noticing that the average values of the PC1 position in the obtained PCA graph showed a linear relationship with each concentration of MB used (Fig. 5b). In Fig. S16 there is also a linear variation of the measured resistance with the concentration of MB for different frequencies. Thus, the positioning of each sample in relation to PC1 can be associated mainly with the increase in electrical resistance measured from the increase in the concentration of MB used.

The limit of detection (LOD) was calculated using the formula $LOD = 3\ \sigma/S$, in which σ is the standard derivation of the measurement performed with the lowest concentration of MB and S is the slope of the calibration curve in Fig. 5b (Mercante et al., 2021). The LOD was calculated to be 2.4 nmol/L, indicating the high sensitivity of the system (Facure et al., 2017). Table S6 shows the comparison of the analytical parameters for different sensing platforms towards MB detection. The LOD obtained in this work is comparable to or even superior to others reported in the literature, indicating the high sensitivity of the NFM@S-A towards MB.

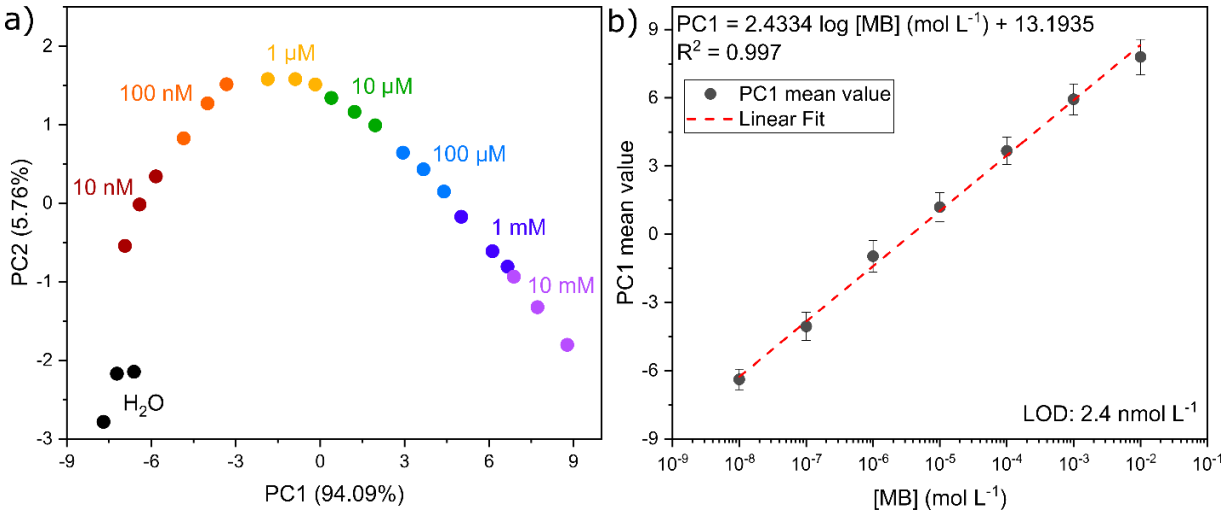

Figure 5. a) PC1 average value versus MB concentration and b) PCA plot for the electrical resistance response.

3.3.3 Hydrogen peroxide electrogeneration

The in situ H_2O_2 generation is an attractive approach to producing this important oxidant, which finds application in the synthesis and production of chemicals disinfection and even for the removal of contaminants from water and wastewater by means of H_2O_2-based advanced oxidation processes (Santos et al., 2022). In the literature, several carbon-based materials have been studied to perform the oxygen reduction reaction via 2-electrons (2e-ORR) mechanism on the cathode surface (Luo et al., 2020).

The NFM@S and NFM@S-A were used due to their electrical conductive characteristics, which was not observed in the NFM/S3%. Firstly, the activated and non-activated NFM membranes were electrochemically characterized by means of linear sweep voltammetry (LSV) (Fig. 6a). As can be observed from LSV curves under O_2 flow, the cathodic current observed for the activated NFM is nearly twice that of the non-activated carbon, which indicates an improved ORR activity for the activated NFM. Moreover, cyclic voltammetries recorded at 50 mV/s in the potential range of -1.0 to 1.2 V vs Ag/AgCl showed that total voltammetric charge of activated NFM is twice that of the non-activated NFM membrane, which indicates that the electrochemical surface area increased after activation (Fig. 6b). This corroborates with SEM images, once after activation the membrane presented expanded porosity, which provides more actives sites for O_2 adsorption and facilitates H_2O_2 electrogeneration at the surface of the cathode.

To evaluate the efficiency of the membranes for H_2O_2 electrogeneration, electrolysis was conducted in 0.1 mol/L K_2SO_4 medium applying a 25 mA/cm during 90 min (Fig. 6c). As expected, the activated NFM membrane (hydrophilic) presented activity for H_2O_2 generation, where the maximum amount of ~25.5 mg/L of this oxidant was obtained. In contrast, employing the non-activated NFM membrane (hydrophobic) the H_2O_2 electrogeneration attained values close to zero. These results corroborate with the electrochemical characterization of the membranes. This behavior can be easily correlated to the greater concentration of oxygen on the soot surface of activated NFM membrane, as observed by XPS analysis (Table 3). The surface oxygenation of NFMs after activation also increases the hydrophilic character of the soot, as previously observed by contact angle measurements (detail in Fig. 1 b and d), which means that the changes on the surface chemistry, induced by the activation of soot, contributes positively for the H_2O_2 production. Other studies in the literature also shows this correlation, for example, the improvement of catalytic activity of commercial carbon Printex L6 and Vulcan carbon XC72R towards 2e-ORR as a function of higher concentrations of oxygenated groups and consequently increased hydrophilic character has been previously reported (Assumpção et al., 2011).

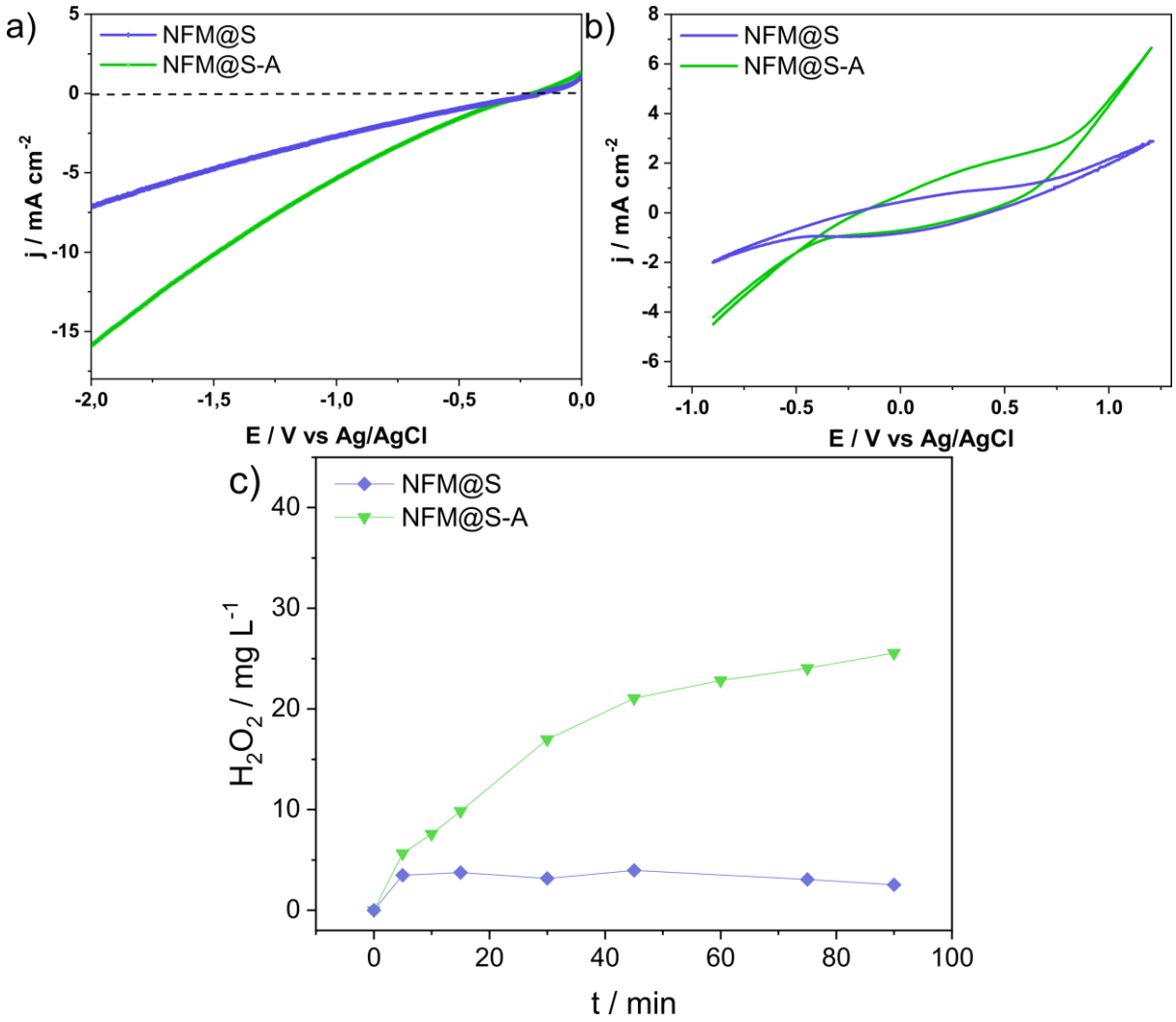

Figure 6. a) Linear sweep voltammetry, b) cyclic voltammetry and c) H_2O_2 generation of NFM@S and NFM@S-A.

3.4 Performance analysis of the multifunctional membranes

An evaluation of nanofibers pre- and post-modified with soot is presented in Fig. 7. The immobilization of soot onto the nanofibrous membrane using pre-synthesis and post-synthesis methods has demonstrated suitability for various applications. However, important issues need to be addressed in future research to improve this immobilization and facilitate the practical applications of the membranes. For instance, the pre-synthesis method exhibited a discontinuous distribution of soot across the nanofibers (Fig. 1a). Furthermore, the presence of formic acid, which is necessary for PA6 solubilization, contributed to soot agglomeration due to its chemical reducing action, posing a challenge to increasing its concentration. Therefore, exploring the use of pre synthesis soot in nanofibers through solubilization in non-acidic solvents is recommended.

In contrast, the post-synthesis method results in soot agglomerates that completely covered the membranes, thereby reducing the available interaction surface. However, activation with NaOH increased the surface area and hydrophilicity of the membranes. Nevertheless, the hydrophobic nature of the inner layers within the soot agglomerates hindered their interaction with water in adsorption process. Conversely, the combination of a hydrophilic surface and a hydrophobic and conductive interior in the soot agglomerates enable their use in sensing and peroxide electrogeneration applications. In addition, the ease of production and the low amount of chemicals employed is economically and environmentally advantageous (Mariana et al., 2021). Hence, it is anticipated that further optimization of the soot and nanofibers combination could yield superior results compared to those obtained in this study. Besides, for future works it would be important to evaluate the NFMs performance varying the conditions of temperature and other target molecules such as heavy metals and other organic pollutants. Furthermore, studies involving soot dispersion in different solvents and solutions are needed.

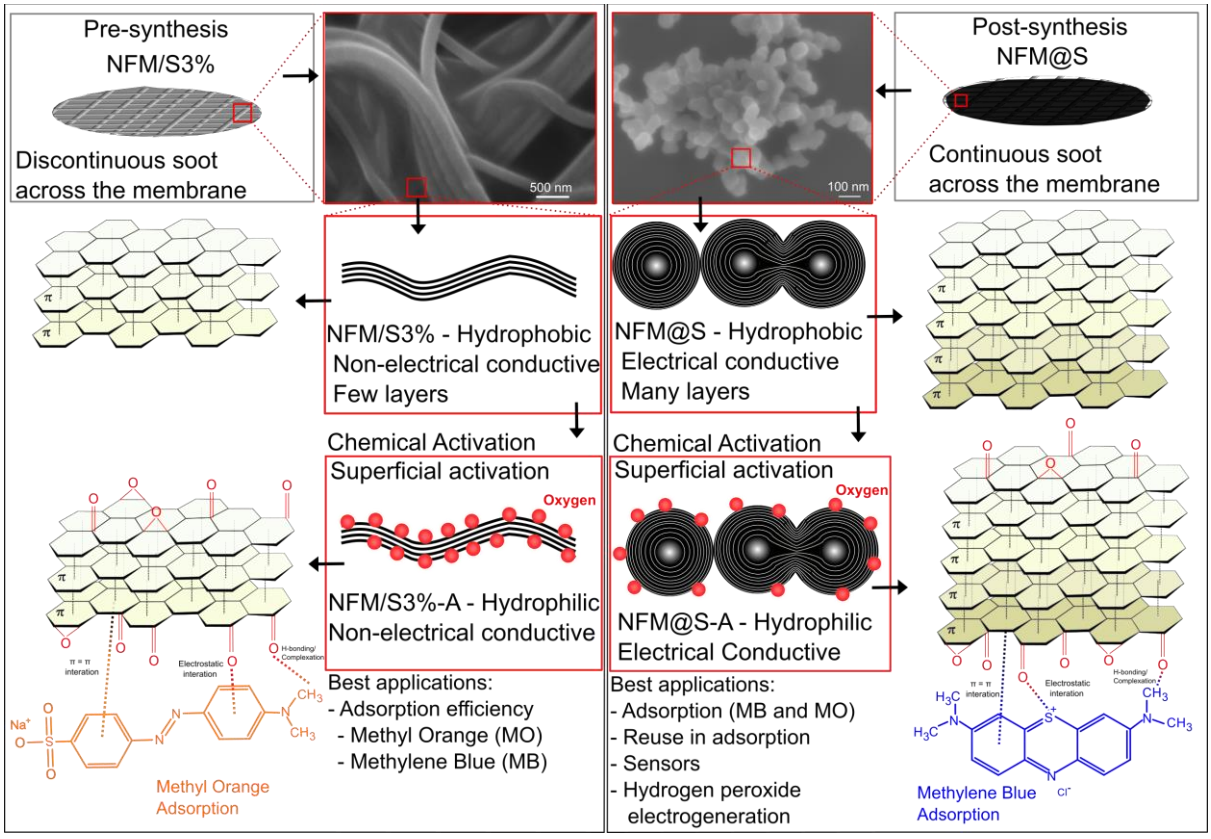

Figure 7: Scheme of the morphology of soot pre and post modified NFMs before and after chemical activation, adsorption mechanism and list of the best performing applications.

4. Conclusions

A novel multifunctional nanofiber membrane produced by solution blow spinning and modified with soot was developed and applied for the adsorption and sensing of cationic dye, as well as in the electrogeneration of H_2O_2. The pre-synthesis method exhibited a notable inclination to prevent soot agglomeration, which can be further enhanced through dispersion in non-acid solvents. In contrast, the post synthesis method retained the agglomeration structure of soot. The chemical activation employed in both methods led to an improvement in the hydrophilicity of the soot. Furthermore, the immobilization of soot was found to be crucial for the successful activation in NaOH solution, as direct dispersion of soot in the solution was hindered by its high hydrophobicity.

The NFM/S3% pre-synthesis approach demonstrated higher effectiveness towards MB adsorption due to its reduced degree of agglomeration. The relative efficiency of adsorption in batch reached (experimentally) 94.33 mg/g and calculated from 37.71 mg/g, while in fixed bed adsorption the efficiency reached 8 mg/g with 60% drop in the 10th cycle of reuse. On the other hand, post-modified NFM showed adsorption efficiency in batch of (experimentally) 74.91 mg/g and calculated from 36.38 mg/g, while in fixed bed the efficiency reached 3.86 mg/g. The discrepancy between the higher experimental efficiency and the calculated efficiency arises from variability in the results, primarily attributed to the heterogeneous activation of the soot surface resulting from its hydrophobic behavior and elevated levels of agglomeration. Although the lower efficiency, the post-modified NFM showed good stability during cyclic MB removal, which can be important to achieve real scale applications. The observed efficiency level of up to 80% for MB removal in 10 mg/L solutions, along with significant reuse capacity, suggests that these NFMs hold promise as potential candidates for reducing the concentration of solutions containing organic pollutants. In addition, the ability to remove cationic and anionic pollutants makes these NFMs candidates to clean up complex water resources in terms of the presence of pollutants varieties. Furthermore, the post-modified NFMs have also been successfully applied in electrodes for MB sensing using impedance spectroscopy, yielding a limit of detection of 2.4 nmol/L. Finally, the dual characteristics observed in the contact angle of post-modified and activated NFM were important to generate hydrogen peroxides as a proof of concept. The synergistic combination of nanomaterials and innovative design strategies holds the key to expanding the potential applications of multifunctional nanofibrous membranes. This approach not only opens new avenues for integrating filtration with other functionalities in membrane technology but also paves the way for the development of next-generation membrane separation processes. Additionally, it

presents a promising opportunity to address the issue of reusing plastic waste residues (resulting from incineration), thereby contributing to a more sustainable and environmentally friendly solution.

Acknowledgements:

The authors thank financial support from Fundação de Amparo à Pesquisa do Estado de São Paulo (FAPESP) [grant numbers: 2018/22214-6, 2014/50945-4, 2017/10118-0, 2017/10582-8, 2020/07351-7, 2020/02743-4], Conselho Nacional de Desenvolvimento Científico e Tecnológico (CNPq) [grant numbers: 445982/2020-9, 351393/2022-6, 381405/2021-4, 303759/2014-3, 303943/2021-1], MCTI-SisNano [grant number: CNPq/402.287/2013-4], Coordenação de Aperfeiçoamento de Pessoal de Nível Superior (CAPES - Brazil) [grant number: 001 - 88882.426501/2019-01], and Rede Agronano (EMBRAPA) from Brazil.

References:

Ali, S., Rehman, S.A.U., Luan, H.Y., Farid, M.U., Huang, H., 2019. Challenges and opportunities in functional carbon nanotubes for membrane-based water treatment and desalination. Sci. Total Environ. 646, 1126–1139. https://doi.org/10.1016/j.scitotenv.2018.07.348

Alvarenga, A.D., Andre, S., Teodoro, K.B.R., Schneider, R., Mercante, L.A., Correa, D.S., 2023. Nanofibrous filtering membranes modified with sucrose-derived carbonaceous materials for adsorption in batch and fixed bed. Chem. Eng. J. 451, 138557. https://doi.org/10.1016/j.cej.2022.138557

Alvarenga, A.D., Correa, D.S., 2021. Composite nanofibers membranes produced by solution blow spinning modified with CO2-activated sugarcane bagasse fly ash for efficient removal of water pollutants. J. Clean. Prod. 285, 125376. https://doi.org/10.1016/j.jclepro.2020.125376

Andre, R.S., Dos Santos, D.M., Mercante, L.A., Facure, M.H.M., Campana-Filho, S.P., Mattoso, L.H.C., Correa, D.S., 2020. Nanochitin-based composite films as a disposable ethanol sensor. J. Environ. Chem. Eng. 8, 104163. https://doi.org/10.1016/j.jece.2020.104163

Assumpção, M.H.M.T., De Souza, R.F.B., Rascio, D.C., Silva, J.C.M., Calegaro, M.L., Gaubeur, I., Paixão, T.R.L.C., Hammer, P., Lanza, M.R.V., Santos, M.C., 2011. A

642 comparative study of the electrogeneration of hydrogen peroxide using Vulcan and
643 Printex carbon supports. Carbon N. Y. 49, 2842–2851.
644 https://doi.org/10.1016/j.carbon.2011.03.014
645 Barros, W.R.P., Reis, R.M., Rocha, R.S., Lanza, M.R.V., 2013. Electrogeneration of
646 hydrogen peroxide in acidic medium using gas diffusion electrodes modified with cobalt
647 (II) phthalocyanine. Electrochim. Acta 104, 12–18.
648 https://doi.org/10.1016/j.electacta.2013.04.079
649 Blanchard, G., Maunaye, M., Martin, G., 1984. Removal of heavy metals from waters by
650 means of natural zeolites. Water Res. 18, 1501–1507. https://doi.org/10.1016/0043-
651 1354(84)90124-6
652 Bohart, G.S., Adams, E.Q., 1920. Some aspects of the behavior of charcoal with respect to
653 chlorine. J. Am. Chem. Soc. 42, 523–544. https://doi.org/10.1021/ja01448a018
654 Bonilla-Petriciolet, A., Mendoza-Castillo, D.I., Reynel-Ávila, H.E., 2017. Adsorption
655 processes for water treatment and purification, Adsorption Processes for Water
656 Treatment and Purification. https://doi.org/10.1007/978-3-319-58136-1
657 Byamba-Ochir, N., Shim, W.G., Balathanigaimani, M.S., Moon, H., 2016. Highly porous
658 activated carbons prepared from carbon rich Mongolian anthracite by direct NaOH
659 activation. Appl. Surf. Sci. 379, 331–337. https://doi.org/10.1016/j.apsusc.2016.04.082
660 Chu, K.H., 2020. Breakthrough curve analysis by simplistic models of fixed bed adsorption:
661 In defense of the century-old Bohart-Adams model. Chem. Eng. J. 380, 122513.
662 https://doi.org/10.1016/j.cej.2019.122513
663 Du, K., Li, J., 2019. Towards a green world: How do green technology innovations affect
664 total-factor carbon productivity. Energy Policy 131, 240–250.
665 https://doi.org/10.1016/j.enpol.2019.04.033
666 Facure, M.H.M., Mercante, L.A., Mattoso, L.H.C., Correa, D.S., 2017. Detection of trace
667 levels of organophosphate pesticides using an electronic tongue based on graphene
668 hybrid nanocomposites. Talanta 167, 59–66.
669 https://doi.org/10.1016/j.talanta.2017.02.005
670 Forti, J.C., Rocha, R.S., Lanza, M.R.V., Bertazzoli, R., 2007. Electrochemical synthesis of
671 hydrogen peroxide on oxygen-fed graphite/PTFE electrodes modified by 2-
672 ethylanthraquinone. J. Electroanal. Chem. 601, 63–67.
673 https://doi.org/10.1016/j.jelechem.2006.10.023
674 Freundlich, H.M.F., 1906. Over the adsorption in solution. J. Phys. Chem 57, 1100–1107.
675 He, Q., Guo, Q., Umeki, K., Ding, L., Wang, F., Yu, G., 2021. Soot formation during

biomass gasification: A critical review. Renew. Sustain. Energy Rev. 139, 110710. https://doi.org/10.1016/j.rser.2021.110710

Jiang, H., Yang, Y., Yu, J., 2020. Application of concentration-dependent HSDM to the lithium adsorption from brine in fixed bed columns. Sep. Purif. Technol. 241, 116682. https://doi.org/10.1016/j.seppur.2020.116682

Karthikeyan, P., Elanchezhiyan, S.S.D., Banu, H.A.T., Hasmath Farzana, M., Park, C.M., 2021. Hydrothermal synthesis of hydroxyapatite-reduced graphene oxide (1D–2D) hybrids with enhanced selective adsorption properties for methyl orange and hexavalent chromium from aqueous solutions. Chemosphere. https://doi.org/10.1016/j.chemosphere.2021.130200

Kirrane, E.F., Luben, T.J., Benson, A., Owens, E.O., Sacks, J.D., Dutton, S.J., Madden, M., Nichols, J.L., 2019. A systematic review of cardiovascular responses associated with ambient black carbon and fine particulate matter. Environ. Int. 127, 305–316. https://doi.org/10.1016/j.envint.2019.02.027

Kumar Sahoo, S., Kumar Sahoo, J., Kumar Panigrahi, G., Kumar Pattanayak, D., Sundar Rout, A., Lenka, A., 2020. Preparation of graphene oxide from Bio-soot wastes: As an efficient adsorbent for highly noxious Congo red dye. FlatChem 24, 100198. https://doi.org/10.1016/j.flatc.2020.100198

Lagergren, S.K., 1898. About the theory of so-called adsorption of soluble substances. Sven. Vetenskapsakad. Handingarl.

Langmuir, I., 1918. The adsorption of gases on plane surfaces of glass, mica and platinum. J. Am. Chem. Soc. 40, 1361–1403. https://doi.org/10.1021/ja02242a004

Li, L., Zhang, D., Deng, J., Gou, Y., Fang, J., Cui, H., Zhao, Y., Cao, M., 2021. Carbon-based materials for fast charging lithium-ion batteries. Carbon N. Y. 183, 721–734. https://doi.org/10.1016/j.carbon.2021.07.053

Li, S., Huang, L., Zhang, H., Huang, Z., Jia, Q., Zhang, S., 2021. Adsorption mechanism of methylene blue on oxygen-containing functional groups modified graphitic carbon spheres: Experiment and DFT study. Appl. Surf. Sci. 540, 148386. https://doi.org/10.1016/j.apsusc.2020.148386

Long, C.M., Nascarella, M.A., Valberg, P.A., 2013. Carbon black vs. black carbon and other airborne materials containing elemental carbon: Physical and chemical distinctions. Environ. Pollut. 181, 271–286. https://doi.org/10.1016/j.envpol.2013.06.009

Luo, Y., Wu, Y., Huang, C., Xiao, D., Zhang, L., Ma, S., Qu, J., Zheng, S., Chu, P.K., 2020. Graphite felt incorporated with MoS2/rGO for electrochemical detoxification of high-

arsenic fly ash. Chem. Eng. J. 382. https://doi.org/10.1016/j.cej.2019.122763
Mariana, M., Abdul, A.K., Mistar, E.M., Yahya, E.B., Alfatah, T., Danish, M., Amayreh, M., 2021. Recent advances in activated carbon modification techniques for enhanced heavy metal adsorption. J. Water Process Eng. 43, 102221. https://doi.org/10.1016/j.jwpe.2021.102221
Mercante, L.A., Andre, R.S., Facure, M.H.M., Fugikawa-Santos, L., Correa, D.S., 2021. Design of a bioelectronic tongue for glucose monitoring using zinc oxide nanofibers and graphene derivatives. Sensors and Actuators Reports 3, 100050. https://doi.org/10.1016/j.snr.2021.100050
Michelsen, H.A., 2017. Probing soot formation, chemical and physical evolution, and oxidation: A review of in situ diagnostic techniques and needs. Proc. Combust. Inst. 36, 717–735. https://doi.org/10.1016/j.proci.2016.08.027
Neolaka, Y.A.B., Lawa, Y., Naat, J., Lalang, A.C., Widyaningrum, B.A., Ngasu, G.F., Niga, K.A., Darmokoesoemo, H., Iqbal, M., Kusuma, H.S., 2023a. Adsorption of methyl red from aqueous solution using Bali cow bones (Bos javanicus domesticus) hydrochar powder. Results Eng. 17, 1–10. https://doi.org/10.1016/j.rineng.2022.100824
Neolaka, Y.A.B., Lawa, Y., Naat, J., Riwu, A.A.P., Lindu, Y.E., Darmokoesoemo, H., Widyaningrum, B.A., Iqbal, M., Kusuma, H.S., 2021. Evaluation of magnetic material IIP@GO-Fe3O4 based on Kesambi wood (Schleichera oleosa) as a potential adsorbent for the removal of Cr(VI) from aqueous solutions. React. Funct. Polym. 166. https://doi.org/10.1016/j.reactfunctpolym.2021.105000
Neolaka, Y.A.B., Lawa, Y., Naat, J., Riwu, A.A.P., Mango, A.W., Darmokoesoemo, H., Widyaningrum, B.A., Iqbal, M., Kusuma, H.S., 2022. Efficiency of activated natural zeolite-based magnetic composite (ANZ-Fe3O4) as a novel adsorbent for removal of Cr(VI) from wastewater. J. Mater. Res. Technol. 18, 2896–2909. https://doi.org/10.1016/j.jmrt.2022.03.153
Neolaka, Y.A.B., Riwu, A.A.P., Aigbe, U.O., Ukhurebor, K.E., Onyancha, R.B., Darmokoesoemo, H., Kusuma, H.S., 2023b. Potential of activated carbon from various sources as a low-cost adsorbent to remove heavy metals and synthetic dyes. Results Chem. 5, 100711. https://doi.org/10.1016/j.rechem.2022.100711
Neolaka, Y.A.B., Supriyanto, G., Kusuma, H.S., 2018. Adsorption performance of Cr(VI)-imprinted poly(4-VP-co-MMA) supported on activated Indonesia (Ende-Flores) natural zeolite structure for Cr(VI) removal from aqueous solution. J. Environ. Chem. Eng. 6, 3436–3443. https://doi.org/10.1016/j.jece.2018.04.053

744 Nwafor, N.P., Moutloali, R.M., Sikhwivhilu, K., Familoni, O.B., Adams, L.A., 2021.
745 Antifouling polyethersulfone-petrol soot nanoparticles composite ultrafiltration
746 membrane for dye removal in wastewater. Membranes (Basel). 11.
747 https://doi.org/10.3390/membranes11050361
748 Pahalagedara, L., Sharma, H., Kuo, C.H., Dharmarathna, S., Joshi, A., Suib, S.L.,
749 Mhadeshwar, A.B., 2012. Structure and oxidation activity correlations for carbon blacks
750 and diesel soot. Energy and Fuels 26, 6757–6764. https://doi.org/10.1021/ef301331b
751 Paulovich, F. V., Oliveira, M.C.F., Minghim, R., 2007. The projection explorer: A flexible
752 tool for projection-based multidimensional visualization. Proc. SIBGRAPI 2007 - 20th
753 Brazilian Symp. Comput. Graph. Image Process. 27–34.
754 https://doi.org/10.1109/SIBGRAPI.2007.21
755 Pratap Singh, V., Vaish, R., 2020. Cement-based diesel exhaust emission soot coatings for
756 the removal of organic pollutants from water. Constr. Build. Mater. 234, 117377.
757 https://doi.org/10.1016/j.conbuildmat.2019.117377
758 Quina, M.J., Bontempi, E., Bogush, A., Schlumberger, S., Weibel, G., Braga, R., Funari, V.,
759 Hyks, J., Rasmussen, E., Lederer, J., 2018. Technologies for the management of MSW
760 incineration ashes from gas cleaning: New perspectives on recovery of secondary raw
761 materials and circular economy. Sci. Total Environ. 635, 526–542.
762 https://doi.org/10.1016/j.scitotenv.2018.04.150
763 Ringnér, M., 2008. What is principal component analysis? Nat. Biotechnol. 26, 303–304.
764 https://doi.org/10.1038/nbt0308-303
765 Sabri, Y.M., Kandjani, A.E., Rashid, S.S.A.A.H., Harrison, C.J., Ippolito, S.J., Bhargava,
766 S.K., 2018. Soot template TiO2 fractals as a photoactive gas sensor for acetone
767 detection. Sensors Actuators, B Chem. 275, 215–222.
768 https://doi.org/10.1016/j.snb.2018.08.059
769 Saini, D., Gunture, N., Kaushik, J., Aggarwal, R., Tripathi, K.M., Sonkar, S.K., 2021. Carbon
770 Nanomaterials Derived from Black Carbon Soot: A Review of Materials and
771 Applications. ACS Appl. Nano Mater. 4, 12825–12844.
772 https://doi.org/10.1021/acsanm.1c02840
773 Santos, G.O.S., Cordeiro-Junior, P.J.M., Sánchez-Montes, I., Souto, R.S., Kronka, M.S.,
774 Lanza, M.R.V., 2022. Recent advances in H2O2 electrosynthesis based on the
775 application of gas diffusion electrodes: challenges and opportunities. Curr. Opin.
776 Electrochem. 36, 101124. https://doi.org/10.1016/j.coelec.2022.101124
777 Santoso, E., Ediati, R., Kusumawati, Y., Bahruji, H., Sulistiono, D.O., Prasetyoko, D., 2020.

778 Review on recent advances of carbon based adsorbent for methylene blue removal from
779 waste water. Mater. Today Chem. 16, 100233.
780 https://doi.org/10.1016/j.mtchem.2019.100233
781 Shen, Y., Li, L., Xiao, K., Xi, J., 2016. Constructing Three-Dimensional Hierarchical
782 Architectures by Integrating Carbon Nanofibers into Graphite Felts for Water
783 Purification. ACS Sustain. Chem. Eng. 4, 2351–2358.
784 https://doi.org/10.1021/acssuschemeng.6b00030
785 Singh, G., Sharma, M., Vaish, R., 2019. Tunable surface adsorption and wettability of candle
786 soot coated on ferroelectric ceramics. J. Adv. Res. 16, 35–42.
787 https://doi.org/10.1016/j.jare.2018.12.005
788 Singh, V.P., Vaish, R., 2020. Tunable adsorption activity of candle soot nanoparticles
789 depending on the flame height. Eng. Res. Express 2. https://doi.org/10.1088/2631-
790 8695/abadd8
791 Sirignano, M., Ghiassi, H., D'Anna, A., Lighty, J.A.S., 2016. Temperature and oxygen
792 effects on oxidation-induced fragmentation of soot particles. Combust. Flame 171, 15–
793 26. https://doi.org/10.1016/j.combustflame.2016.05.011
794 Tran, H.N., You, S.J., Hosseini-Bandegharaei, A., Chao, H.P., 2017. Mistakes and
795 inconsistencies regarding adsorption of contaminants from aqueous solutions: A critical
796 review. Water Res. https://doi.org/10.1016/j.watres.2017.04.014
797 Trubetskaya, A., Kling, J., Ershag, O., Attard, T.M., Schröder, E., 2019. Removal of phenol
798 and chlorine from wastewater using steam activated biomass soot and tire carbon black.
799 J. Hazard. Mater. 365, 846–856. https://doi.org/10.1016/j.jhazmat.2018.09.061
800 Wan, H., Cao, Y., Lo, L.W., Zhao, J., Sepúlveda, N., Wang, C., 2020. Flexible Carbon
801 Nanotube Synaptic Transistor for Neurological Electronic Skin Applications. ACS Nano
802 14, 10402–10412. https://doi.org/10.1021/acsnano.0c04259
803 Wang, Q., Zhang, F., Li, R., Li, L., 2022. The impact of renewable energy on decoupling
804 economic growth from ecological footprint – An empirical analysis of 166 countries. J.
805 Clean. Prod. 354, 131706. https://doi.org/10.1016/j.jclepro.2022.131706
806 Wang, S., Ma, Q., Zhu, Z.H., 2008. Characteristics of coal fly ash and adsorption application.
807 Fuel 87, 3469–3473. https://doi.org/10.1016/j.fuel.2008.05.022
808 Wang, Y., Zhang, L., Hou, H., Xu, W., Duan, G., He, S., Liu, K., Jiang, S., 2021. Recent
809 progress in carbon-based materials for supercapacitor electrodes: a review. J. Mater. Sci.
810 56, 173–200. https://doi.org/10.1007/s10853-020-05157-6
811 Yan, J., Dong, K., Zhang, Y., Wang, X., Aboalhassan, A.A., Yu, J., Ding, B., 2019.

Multifunctional flexible membranes from sponge-like porous carbon nanofibers with high conductivity. Nat. Commun. 10, 1–9. https://doi.org/10.1038/s41467-019-13430-9

Yao, X., Guo, Z., Liu, Y., Li, J., Feng, W., Lei, H., Gao, Y., 2019. Reduction potential of GHG emissions from municipal solid waste incineration for power generation in Beijing. J. Clean. Prod. 241, 118283. https://doi.org/10.1016/j.jclepro.2019.118283

Ye, N., Cimetiere, N., Heim, V., Fauchon, N., Feliers, C., Wolbert, D., 2019. Upscaling fixed bed adsorption behaviors towards emerging micropollutants in treated natural waters with aging activated carbon: Model development and validation. Water Res. 148, 30–40. https://doi.org/10.1016/j.watres.2018.10.029

Yuan, X.T., Xu, C.X., Geng, H.Z., Ji, Q., Wang, L., He, B., Jiang, Y., Kong, J., Li, J., 2020. Multifunctional PVDF/CNT/GO mixed matrix membranes for ultrafiltration and fouling detection. J. Hazard. Mater. 384, 120978. https://doi.org/10.1016/j.jhazmat.2019.120978

Yuh-Shan, H., 1995. ADSORPTION OF HEAVY METALS EROM WASTE STREAMS BY PEAT School of Chemical Engineering 130–137.

Zhang, Z., Hao, J., Yang, W., Lu, B., Tang, J., 2015. Modifying candle soot with FeP nanoparticles into high-performance and cost-effective catalysts for the electrocatalytic hydrogen evolution reaction. Nanoscale 7, 4400–4405. https://doi.org/10.1039/c4nr07436j

Zhao, R., Wang, Y., Li, X., Sun, B., Li, Y., Ji, H., Qiu, J., Wang, C., 2016. Surface Activated Hydrothermal Carbon-Coated Electrospun PAN Fiber Membrane with Enhanced Adsorption Properties for Herbicide. ACS Sustain. Chem. Eng. 4, 2584–2592. https://doi.org/10.1021/acssuschemeng.6b00026

Zhao, T., Chen, L., Wang, P., Li, B., Lin, R., Abdulkareem Al-Khalaf, A., Hozzein, W.N., Zhang, F., Li, X., Zhao, D., 2019. Surface-kinetics mediated mesoporous multipods for enhanced bacterial adhesion and inhibition. Nat. Commun. 10, 1–10. https://doi.org/10.1038/s41467-019-12378-0